JACS
JOURNAL OF THE AMERICAN CHEMICAL SOCIETY
Article
pubs.acs.org/JACS

Structural Evolution of 2D Microporous Covalent Triazine-Based Framework toward the Study of High-Performance Supercapacitors

Long Hao,[†,‡] Jing Ning,[†,‡] Bin Luo,[†] Bin Wang,[†] Yunbo Zhang,[†,‡] Zhihong Tang,[∥] Junhe Yang,[∥] Arne Thomas,[⊥] and Linjie Zhi*[,†,∥]

[†]National Center for Nanoscience and Technology, Zhongguancun, Beiyitiao No.11, Beijing 100190, P. R. China
[‡]University of Chinese Academy of Sciences, Beijing 100039, P. R. China
[∥]University of Shanghai for Science and Technology, Jungong Road 516, 200093, Shanghai P.R. China
[⊥]Department of Chemistry, Functional Materials, Technische Universität Berlin, Hardenberg strasse 40, 10623 Berlin, Germany

Supporting Information

ABSTRACT: A series of nitrogen-containing micropore-donimated materials, porous triazine-based frameworks (PTFs), are constructed through the structural evolution of a 2D microporous covalent triazine-based framework. The PTFs feature predictable and controllable nitrogen doping and pore structures, which serve as a model-like system to more deeply understand the heteroatom effect and micropore effect in ionic liquid-based supercapacitors. The experimental results reveal that the nitrogen doping can enhance the supercapacitor performance mainly through affecting the relative permittivity of the electrode materials. Although microspores' contribution is not as obvious as the doped nitrogen, the great performances of the micropore-dominated PTF suggest that micropore-dominated materials still have great potential in ionic liquid-based supercapacitors.

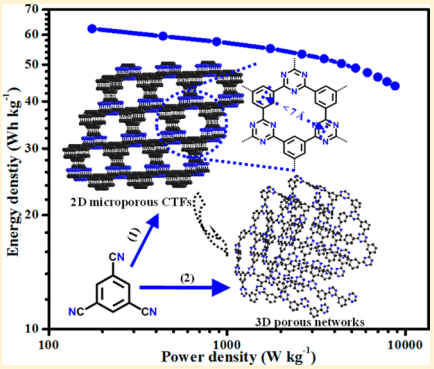

INTRODUCTION

As energy storage devices, supercapacitors have attracted extensive attention due to their high power density, excellent reversibility, and broad operating temperature range.[1−3] However, the low energy density of traditional carbon-based supercapacitors (mostly less than 6 Wh/kg in commercially available supercapacitors) has significantly limited their further application in primary power sources.[4,5] According to the equation $E = {}^1/_2CV^2$, the energy density (E) of a supercapacitor depends on its nominal voltage (V) and the capacitance (C). Since V is mainly limited by the electrolyte stability, consequently, ionic liquid-based electrolytes have been recently investigated, so that the voltage window of the devices can be extended to over 3 V.[6−8] The factor C is generally controlled by the carbon/electrolyte interface. Therefore, rational designing new carbonaceous materials and optimizing their surface structures/functionality have become a major research focus in this field, such as the development of materials with different modalities,[9−11] the investigation of the effective surface area,[12,13] the adjustment of pore size distribution,[14,15] and the introduction of heteroatoms into the carbon skeletons.[16−18]

Among the above efforts to improve the capacitance, two of them have attracted more attention in the past few years. The first is the heteroatom effect (HAE).[19−21] For instance, the doping of nitrogen atoms can affect the electron distribution of the carbon materials, and therefore further enhance the wettability and the electro-active surface area of the electrode,[22,23] besides the active nitrogen atom can also introduce pseudocapacitance to the system (for aqueous supercapacitors),[24−26] which are all beneficial for enhancing the supercapacitor performance. The second effect is the micropore effect (MPE),[14,27] for which many research works including experimental results and theoretical calculations reveal that certain kinds of micropores, especially those with the same size of the electrolyte ions (normally 0.7−1.0 nm, also can be called "subnanopores") in the electrode can contribute significantly to the capacitance of ionic liquid-based supercapacitors.[28−31] The MPE is attractive also because it is somehow conflictive to the tranditional point of view in supercapacitors, in which micropores are believed to barely contribute to the capacitance since the electrolyte ions are unable to enter these pores.[32,33] However, a detailed study of these two effects is very difficult since the heteroatoms and micropores in the commonly selected electrode materials (such as activated carbons, functionalized carbon nanotubes, reduced graphene oxides, and carbonized chain-like/irregularly cross-linked polymers) are not controllable. In the viewpoint of chemistry, a reasonable strategy to deeplier study these effects is to construct model structures consisting of defined heteroatoms and/or pore size distributions, which will be beneficial for a better understanding of the HAE and/or MPE, and consequently to enhance the performance of the supercapacitors.

Received: September 3, 2014
Published: December 15, 2014

DOI: 10.1021/ja508693y
J. Am. Chem. Soc. 2015, 137, 219−225

The development of microporous polymer networks (MPNs) provides a great opportunity for chemically constructing such a material. MPNs are 2D/3D reticular materials built by polymerization of rigid organic molecules, called tectons with functional groups pointing into two or three dimensions.[34−39] Heteroatoms can be controllably introduced into the networks of the materials by using heteroatom-containing molecular building blocks,[40−44] and materials with defined pore sizes can be obtained by selecting molecules with different sizes.[36,45−47] Notably, MPNs usually have high specific surface area and abundant micropores, which should be quite favorable for enhancing the supercapacitor performance when they are applied as electrode materials in supercapacitors. However, MPNs show relatively low conductivity, and therefore the successful examples of investigating MPN-related materials as electrode materials for supercapacitors remain scarce.[48] Nevertheless, in our recent work, we realize that the conductivity problem can be solved by selecting MPNs with conjugated structures and increasing the polymerization temperature, during which time the conductivity is increased significantly, while the basic network skeletons of MPNs are maintained.[49,50]

Herein, we choose a trigonal-symmetrical nitrogen-containing monomer (1, 3, 5-tricyanobenzene) as the building block, which can be used to construct a conjugated microporous covalent triazine-based framework (CTF) through the trimerization reactions (Scheme 1a).[43,51−53] Interestingly,

Scheme 1. (a) The Fundamental Trimerization Reactions of Cyano Groups for Building the Structures Described Herein, and (b) Illustration of the Design and Synthesis of Materials, Including (1) Low-Temperature Construction of 2D Microporous CTF (m-CTF), (2) High-Temperature Synthesis of 3D Nitrogen-Containing Porous Triazine-Based Frameworks (PTFs), and the Structural Evolution from m-CTF Self-Template to PTFs

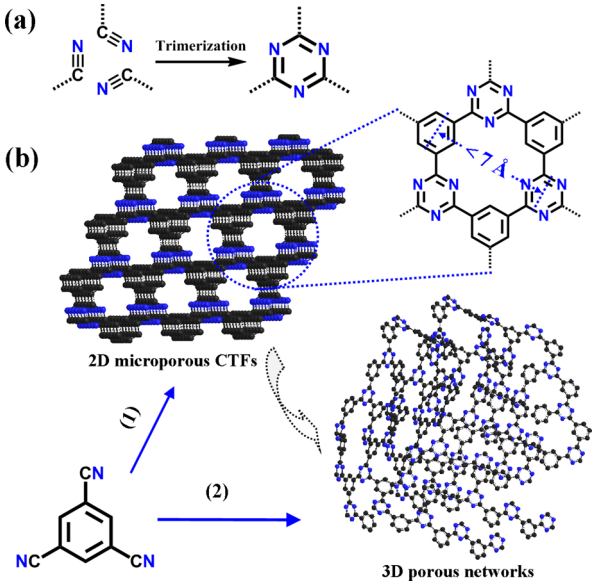

based on this CTF with well-defined nitrogen incorporation and pore size distribution, further structural evolution of this CTF at higher temperatures leads to a CTF-based graphenal polymer[54] with significantly enhanced conductivity but still defined nitrogen incorporation and microporosity, which provides a reasonable model-like system for investigating the influence of heteroatom doping and pore structure to the electrochemical performance and consequently to gain a deeper understanding of the HAE and the MPE in supercapacitors. Specifically, high-voltage supercapacitors with ionic liquid as electrolyte are studied, in which the HAE and MPE are different from that of aqueous supercapacitors.

RESULTS AND DISCUSSION

In order to ensure that the basic structure of this material resemble the one drawn in Scheme 1b(1) (constructed by trimerization reactions only), the polymerization is first carried out at relatively low temperature of 400 °C (ionothermal reactions, see details in Experimental Section),[43,53,55] and the as-prepared material is marked as m-CTF (short for microporous-CTF).

The infrared (IR) spectroscopy and X-ray photoelectron spectroscopy (XPS) are first performed to characterize the nitrogen-contained chemical structure of m-CTF, and a small molecule with similar structure, 2,4,6-triphenyltriazine, is selected as a control sample (Figure 1a). IR spectroscopy of

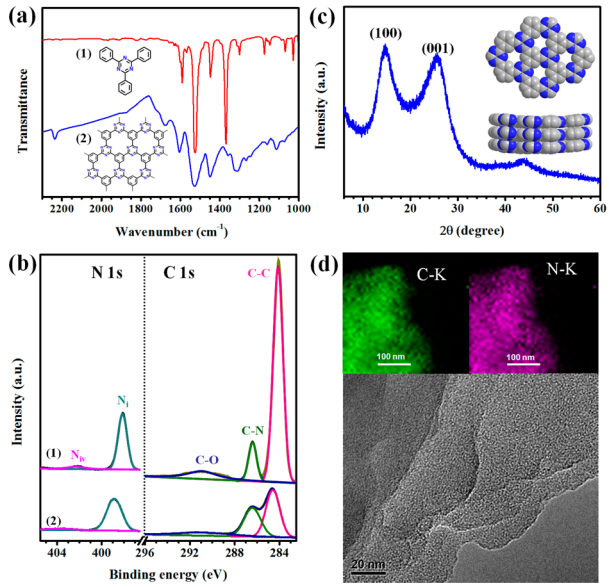

Figure 1. Structural characterization of m-CTF. (a) IR spectra and (b) XPS spectra of m-CTF and the control sample, 2,4,6-triphenyltriazine. (c) XRD pattern of m-CTF with its structural models inserted. (d) Typical TEM image with elemental mapping images inserted.

m-CTF and the control sample (Figure 1a) show similar signals at ∼1520, ∼1440, and ∼1300 cm^{-1}, indicating the existence of triazine and benzene structures in both materials.[45,51] The C 1s deconvolution peaks (XPS results in Figure 1b) at ∼284.4 and ∼286.3 eV demonstrate that both materials possess two kinds of carbons corresponding to C−C and C−N, respectively. Furthermore, N 1s deconvolution peaks (Figure 1b) at ∼398 eV indicate that only one type of nitrogen corresponding to the pyridinic nitrogen (N_i) in triazine rings is present in both materials.[56,57]

Besides the above chemical structure information on m-CTF, its microstructure especially the pore structure is interesting as well. The powder X-ray diffraction (P-XRD) pattern of m-CTF (Figure 1c) shows two broad peaks, suggesting the existence of partially crystalline structures. The peaks at 14° and 26° can be assigned to the in-plane reflection (100) and the vertical

DOI: 10.1021/ja508693y
J. Am. Chem. Soc. 2015, 137, 219−225

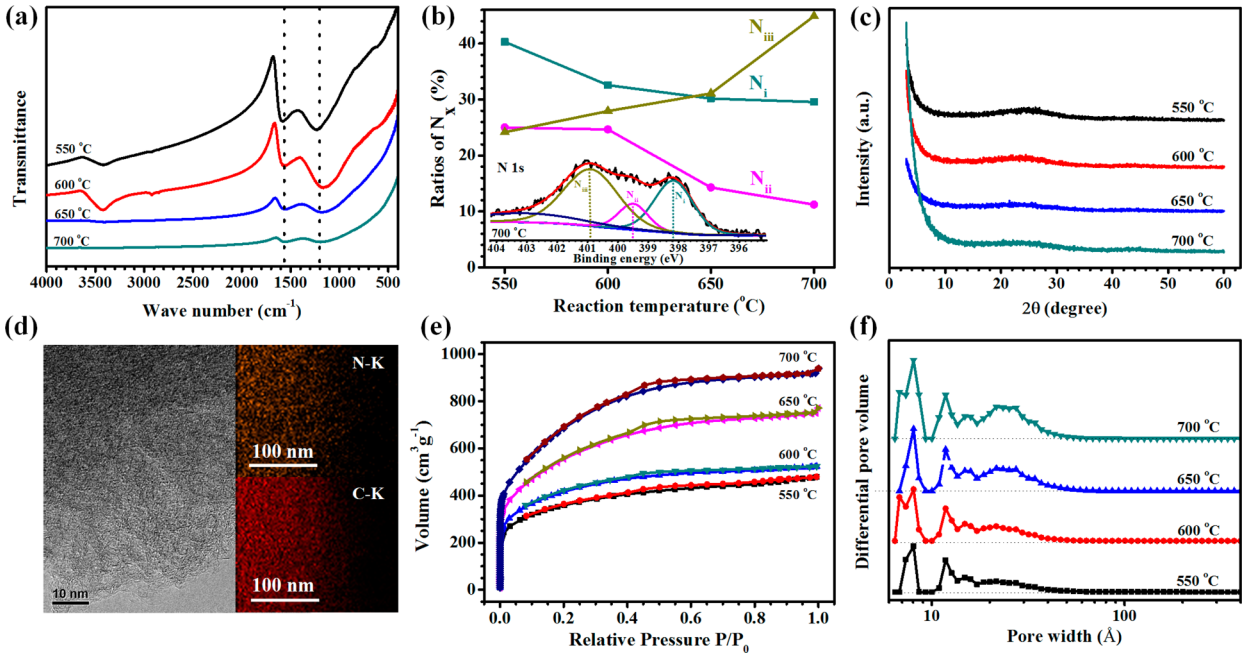

Figure 2. Structural characterization of PTFs. (a) IR spectra. (b) The ratios of different nitrogen configurations determined from the XPS N 1s deconvolution results with typical N 1s deconvolution of PTF-700 inserted. (c) XRD patterns. (d) Typical TEM image and elemental mapping images of PTF-700. (e) Nitrogen adsorption−desorption isotherms. (f) Pore size distributions.

spacing between stacked sheets (001), respectively (see the inserted structural model in Figure 1c), which indicates that m-CTF contains subnanopores smaller than 7 Å. In addition, transmission electron microscopy (TEM, Figure 1d and Figure S1) and atomic force microscopy (AFM, Figure S2) analyses demonstrate the layered structure of m-CTF.

In summary, m-CTF is a 2D, nitrogen-rich microporous framework. At this point, it can be imaged that the structural evolution of this 2D structure into a 3D architecture via cross-linking reactions between the stacked sheets (Scheme 1b) would not only extend the π-conjugated system so that the conductivity of the material could be significantly improved, but also tune the edge structures of the framework and the pore surfaces, which both will be favorable for the enhancement of the supercapacitor performance. Based on this assumption, the trimerization temperature of 1,3,5-tricyanobenzene is increased from 400 to 550−700 °C (see details in the Experimental Section), and the as-prepared materials are named as porous triazine-based frameworks (PTFs) at the given temperature, such as PTF-550, PTF-600, PTF-650, and PTF-700.

Compared with m-CTF, the detailed structure signals of PTFs (IR in Figure 2a) have disappeared only showing the stretching/deformation vibration signals (~1580 and ~1220 cm^{-1}) of benzene/triazine and the overall signal intensity decreases with the increase of the polymerization temperature, which suggests that further cross-linking reactions have occurred and the structures have evolved into a typical graphenal polymer.[54] XPS analysis demonstrates the nitrogen configurations of N 1s (inset in Figure 2b, see also Figure S3 for details) evolve from one kind, pyridinic nitrogen/N_i in m-CTF (Figure 1b) to three kinds in PTFs, including still the pyridinic nitrogen/N_i in triazine rings at ~398.2 eV but also pyrrolic nitrogen (N_{ii}) at ~399.5 eV and quaternary nitrogen (N_{iii}) at ~400.8 eV,[58,59] suggesting the formation of graphitized fragments. In addition, quantitative analysis of XPS suggests that with the increase of the reaction temperatures, the ratios of N_{iii} in PTFs gradually increase while the ratios of N_i and N_{ii} decrease (Figure 2b and details in Table S1),[60,61] which also confirms the occurring of further cross-linking reactions/rearrangement reactions and the gradual increase of graphitized fragments under higher temperatures.

Interestingly, further cross-linking/rearrangement reactions induced by high temperature also cause evolution of the pore structures in PTFs. The XRD patterns of PTFs reveal no distinguishable peaks (Figure 2c), indicating that PTFs have turned into amorphous structures. The TEM images (Figure 2d, see also Figure S4) show that extremely abundant pores have emerged, while elemental mapping demonstrates there are still homogeneously distributed nitrogen atoms. The nitrogen adsorption/desorption measurements disclose that PTFs prepared at lower temperatures (Figure 2e) show type I isotherms. However, as the polymerization temperature increases, an increasing uptake at higher relative pressures is observed, which suggests that beside the large amount of micropores, mesopores tend to appear with the increasing temperature. Evaluation of the pore size distribution based on the density functional theory (DFT) further verifies this finding (Figure 2f). In addition, the BET surface areas of PTFs increase from 1212 to 2482 m^2/g when the reaction temperatures are changed from 550 to 700 °C (Table S2).

All the above characterizations demonstrate that the 2D microporous m-CTF has been successfully evolved into a 3D nitrogen-containing micropore-dominated framework via the increase of reaction temperatures. More importantly, the PTFs maintain their intrinsic nitrogen-doping and controllable microporous structures, as well as high surface areas, abundant pore structures, and extended π-conjugated systems, which make them a reasonable model-like structure for studying the HAE and MPE in ionic liquid-based supercapacitors.

The supercapacitor performances of these model-like structures are then evaluated by a conventional two-electrode symmetric supercapacitor system (a coin-type cell of 2032

DOI: 10.1021/ja508693y
J. Am. Chem. Soc. 2015, 137, 219−225

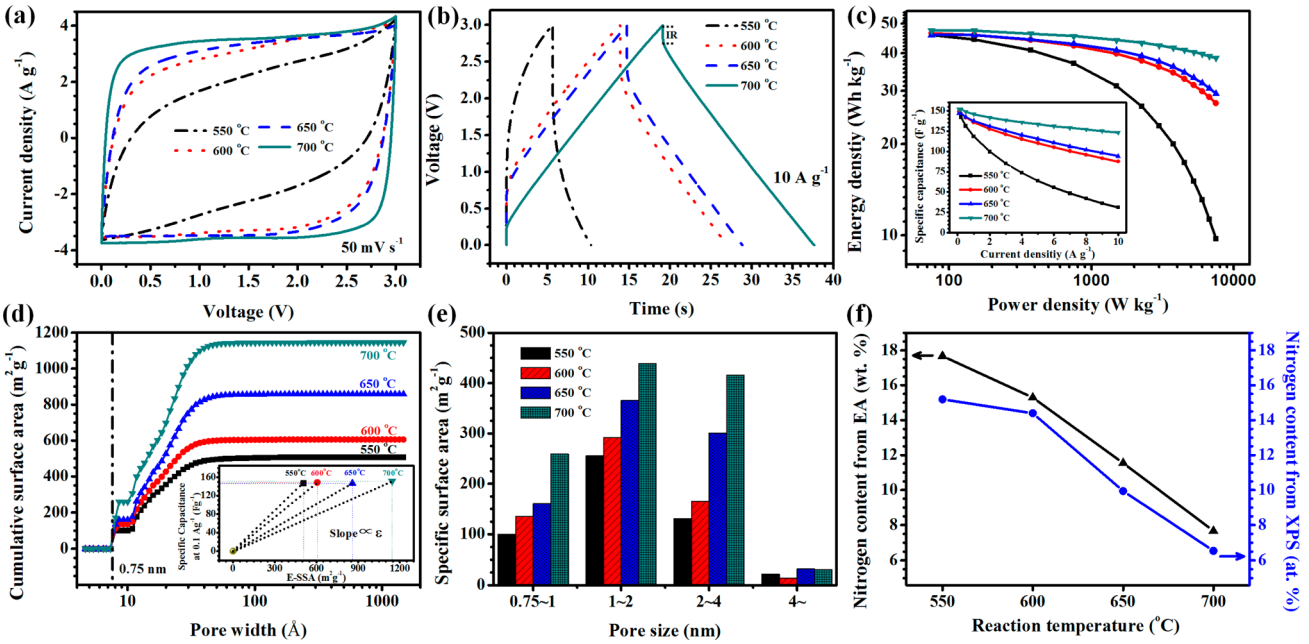

Figure 3. (a–c) Electrochemical properties of the PTFs: (a) typical CV curves, (b) typical galvanostatic charge–discharge curves, and (c) Ragone plots with specific capacitances at various current densities inserted. (d–f) Further analysis of the causes of the different performances between PTFs prepared at different temperatures: (d) Cumulative density functional theory (DFT) specific surface area (SSA) of PTFs with pore size larger than the ion diameter of the electrolyte (effective SSA, E-SSA); the inset is the specific capacitance at 0.1 A/g versus the E-SSA, and slopes of the lines are proportional to the relative permittivity ε (based on $C = \varepsilon S/d$). (e) DFT SSA distribution of different pore size ranges. (f) Nitrogen contents of the PTFs prepared at different temperatures from EA (wt%) and XPS (at%).

size)[6] with a room temperature ionic liquid ($EMIMBF_4$) as the electrolyte (see details in the Experimental Section). The cyclic voltammetry (CV) curves are first performed from 0 to 3 V at different scan speeds (Figure 3a, and Figure S5 for details). At 10 mV/s, the CV curves of all PTFs display quasi-rectangular shape, corresponding to the decent capacitive character; while at 50 and 100 mV/s, only CV curves of PTFs prepared at 700 °C (PTF-700) can maintain the quasi-rectangular shape, and CV curves of PTF-650, PTF-600, and PTF-550 are gradually changed to fusiform shape, suggesting that PTFs prepared at higher temperatures have better rate capabilities. In addition, the CV curves of PTFs prepared at higher temperatures also have larger integrated area within the potential window, which implies that the specific capacity is higher.

Galvanostatic charge–discharge experiments are then carried out at different current densities from 0.1 to 10 A/g to further characterize their performances. When the current density is lower than 1 A/g, the charge–discharge curves of all the PTFs (Figure S6) show nearly triangular shapes, similar to that of theoretical electrochemical double layer capacitors. As the current density grows up to 10 A/g, only PTF-700 can preserve a triangular shape (Figure 3b), suggesting that PTF-700 has the best rate capability. This is mainly because the conductivity of the material becomes better (voltage drop decreases, IR-drop in Figure 3b) with the increase of the reaction temperature, which can be further confirmed by electrochemical impedance spectroscopy (EIS) testing results in Figure S7.[56] The overall performances of PTFs-based supercapacitors are summarized in Figure 3c (the specific capacitances are extracted from the discharge slopes, see Experimental Section for details). It reveals that PTFs synthesized at higher temperatures have better rate capability and relatively higher capacitive property, which is well consistent with the above CV results. The highest energy density and power density are 47.4 Wh/kg and 7500 W/kg respectively, which are obtained from a PTF-700 based supercapacitor at a working voltage of 3 V (see the Ragone plots in Figure 3c). The cycling stability of the PTF-700 based supercapacitor has also been tested by the galvanostatic charge–discharge measurement at a current density of 10 A/g (Figure S8); and the specific capacitance retains ~85% and the charge–discharge curves maintain triangular even after 10 000 cycles, demonstrating the outstanding stability of the device.

The first test of this PTF-based model in supercapacitor results in attractive performances. However, the insight of the different performances of PTFs caused by the changes of the reaction temperature should be more interesting.

As mentioned above, the decreasing of the voltage drop (IR-drop in Figure 3b) and the EIS analyses (Figure S7) have elucidated that higher polymerization temperatures lead to better conductivity of the materials which finally results in better rate capability. Nevertheless, there is still one question which needs to be answered. When the reaction temperature climbs from 550 to 700 °C, the specific surface area (SSA) increases dramatically from 1212 to 2482 m^2/g (Table S1), however, the specific capacitances of the corresponding materials are almost unchanged (the specific capacitance only changes from 147.1 to 151.3 F/g at a current density of 0.1A/g, Figure 3c). According to the basic principle of electrochemical double layer capacitors, the capacitance (C) is stored everywhere on the electrode surface and is dependent on the electro-active surface area (S) of the electrode: $C = \varepsilon S/d$, where ε is the relative permittivity, and d is the thickness of the doublelayer (a value of a few angstroms, depending only on the electrolytes ions and the solvent dimensions).[58,62] Normally, only the pores bigger than the diameter of the ions in the electrolyte are useful in a supercapacitor. Herein, solvent-free ionic liquid $EMIMBF_4$ was used as the electrolyte, whose

DOI: 10.1021/ja508693y
J. Am. Chem. Soc. 2015, 137, 219–225

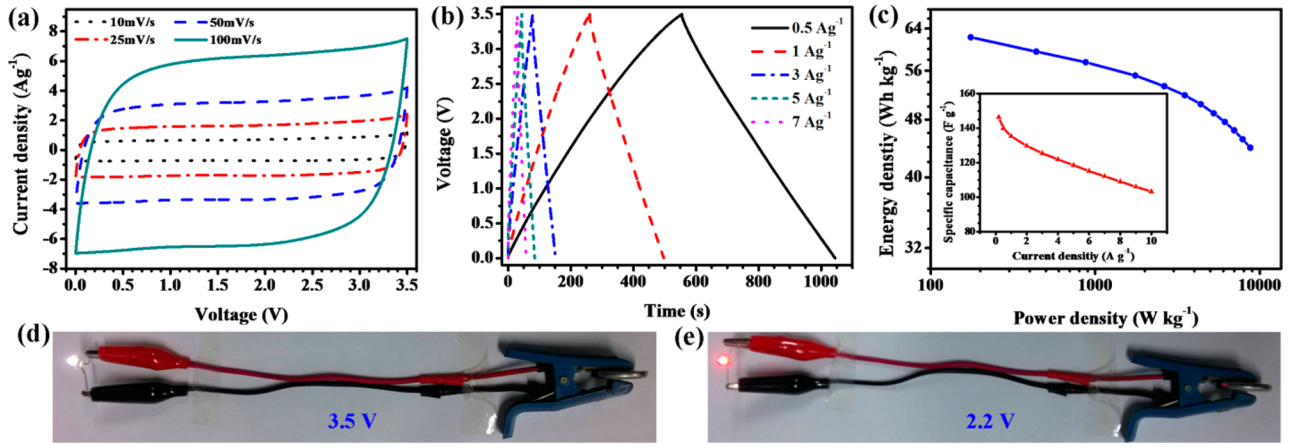

Figure 4. Electrochemical characterizations of PTF-700-based supercapacitors at wider voltage of 3.5 V: (a) CVs, (b) galvanostatic charge−discharge curves, and (c) Ragone plots with specific capacitances inserted. (d,e) The supercapacitor can drive a commercial white LED at 3.5 V and red LED when the voltage dropped to 2.2 V.

biggest ion is $EMIM^+$ with a diameter of 0.75 nm. Therefore, the cumulative density functional theory (DFT) SSAs with pore sizes larger than 0.75 nm are further extracted as the effective SSA (E-SSA, which is the "S" in the above formula) of a supercapacitor (Figure 3d).[12,13] It is observed that the E-SSAs are increasing from 508 to 1145 m^2/g with rising the polymerization temperatures from 550 to 700 °C. Combined with the electrochemical testing results, four curves can be obtained for the specific capacitances of PTFs (at the current density of 0.1 A/g) versus their E-SSAs (inset in Figure 3d). It can be recognized that the specific capacitances of PTFs are not directly related to their E-SSAs but are different for PTFs synthesized at various temperatures. Based on the above equation, $C = \varepsilon S/d$, the slopes of the lines (ε/d) are proportional to the relative permittivity (ε), and consequently, ε is not constant for the PTFs but becomes smaller as the reaction temperature increases ($\varepsilon_{700} < \varepsilon_{650} < \varepsilon_{600} < \varepsilon_{550}$), which suggests that the interaction between the electrolyte and the PTFs prepared at higher temperatures is weaker than at lower temperatures.

Normally, at the same testing conditions, the ε only depends on the intrinsic properties of the electrode materials. In this model-like system, the main differences between PTFs prepared at diverse temperatures are not only their pore sizes but also the refined surface structures and functionality due to the nitrogen-doped features. Consequently, the pore size distributions and the nitrogen contents of PTFs was quantitatively analyzed, which is obviously needed for deeper understanding the influence of MPE and HAE to the ε.

The DFT SSA distribution of different pore sizes (Figure 3e) shows that most of the pores in PTFs are smaller than 4 nm. Notably, the E-SSAs derived from the pores with the size ranges of 0.75−1, 1−2, and 2−4 nm all increase with the reaction temperature. Considering the increase of micropores (including subnanopores) and the decrease of ε, it can be seen that the micropore/subnanopore's contribution to the capacitance is not very obvious, which means in this model-like system the influence of the MPE to the ε is not apparent.

On the other hand, quantitative analyses of nitrogen atoms based on both the elemental analyses and the XPS characterizations (Figure 3f) show that the nitrogen contents in PTFs drop rapidly with increase of the reaction temperatures, which suggests that the electro-active surface functionalities of the material have been dramatically lost along with the raise of the temperatures. As mentioned in the beginning, nitrogen doping can enhance the wettability and the electro-active surface area of the electrode (HAE). Consequently, in this model-like system, the severe drop of nitrogen content can be the dominant factor causing the decrease of ε under higher reaction temperatures. Additionally, the changes of different nitrogen configurations with the reaction temperatures (Figure 2b) also reflect the polymerization/carbonization degree in these model-like structures, which could also affect their surface structure and finally influence the ε.

Obviously, the increase of reaction temperature results in the improvement of the conductivity of the materials (Figure 3b and Figure S7), which leads to the significant enhancement of the rate capability of the electrodes (Figure 3c); while the drop of nitrogen content at higher reaction temperatures (Figure 3f) leads to the reducing of the surface functionality of the material (HAE), which causes the decrease of relative permittivity (ε), and further results in almost no increase in capacitance although the specific surface area is doubled. In short, based on this model electrode material, we have achieved a much deeper understanding of the influencing factors of the specific capacitances, which is quite difficult to obtain from other conventional electrode systems.

Considering that the energy density of a supercapacitor is also limited by the nominal voltage and based on recent reports, the electrolyte used here can also be applied over 3 V.[5] Consequently, a supercapacitor based on PTF-700 was further tested with a voltage increased to 3.5 V. The CV curves of this supercapacitor are all quasi-rectangular even at the scan speed of 100 mV/s (Figure 4a), and all the galvanostatic charge−discharge curves at different current densities reveal nearly isosceles-triangular shape (Figure 4b, see also Figure S9 for details), which indicates their excellent double layer capacitor performance. Figure 4c shows the overall supercapacitor performances, and the highest energy density and power density are 62.7 Wh/kg and 8750 W/kg, respectively, which is comparable to most of the advanced systems reported in the literatures (Figure S10).[6,14,27,59,63−70] In addition, the preparation method of these triazine-based materials is much easier than the reported materials, and more interestingly, their structures can be further tuned by selecting different kinds of monomers or changing the reaction procedures, which provides

DOI: 10.1021/ja508693y
J. Am. Chem. Soc. 2015, 137, 219−225

a versatile reservoir for developing mass producible electrode materials for practical applications in ionic liquid-based supercapacitors.

In order to intuitively manifest the performance of this high voltage supercapacitor, the PTF-700-based supercapacitor was also tested to drive commercial light-emitting diodes (LEDs, see the video in the Supporting Information). It can be seen that it can successfully drive a commercial white LED when being charged to 3.5 V (Figure 4d) and also a commercial red LED when its voltage dropped to 2.2 V (Figure 4e).

By combining the above supercapacitor performance of PTF-700 with its pore size distribution (Figure 3e), it can be seen that PTF-700 contains 61.0% micropores and 97.3% pores smaller than 4 nm, but still shows highly attractive supercapacitor performance including both nice capacitive properties and excellent rate capabilities, which suggests that these micropore-dominated materials have great potential in ionic liquid electrolyte-based supercapacitors. In other words, it may be unnecessary to design and synthesize materials with too many mesopores/macropores, so that the void volume in the materials can be decreased and the volumetric energy density of the supercapacitors can be significantly enhanced. Instead, micropore-dominant materials should be paid much attention in the studies of ionic liquid-based supercapacitors.

CONCLUSIONS

In summary, we have successfully developed a series of nitrogen-contained micropore-donimated structures, PTFs through the structural evolution of a 2D microporous covalent triazine-based framework (m-CTF). The PTFs feature predictable and controllable nitrogen doping and pore structures, serving as a great model-like system to more deeply understand the heteroatom effect (HAE) and micropore effect (MPE) in high-voltage ionic liquid-based supercapacitors, which is extremely important for developing high performance supercapacitors. Experimental investigations disclose that the HAE is extremely significant to the supercapacitors, which reflects the changes of chemical composition and surface functionality during the structural evolution of m-CTF, and it has great influence to the relative permittivity (ε) of the electrode materials. Although the MPE is not that obvious as the HAE in this model-like system, the excellent electrochemical performance of the micropore-dominated electrode, PTF-700, suggests that the micropore-dominated materials indeed have great potential in ionic liquid-based supercapacitors. In addition, the rational design of electrode structures via bottom-up strategies developed in this work opens up a new avenue to deeply understand the electrochemical mechanisms in energy storage devices as well as better design high performance electrode materials for practical applications.

EXPERIMENTAL SECTION

Synthesis of the Precursor, m-CTF, and PTFs. The precursor, 1,3,5-tricyanobenzene was prepared based on the existing report[71] (details in Supporting Information).

m-CTF. m-CTF was synthesized at 400 °C with $ZnCl_2$ as catalysis and solvent at the same time. Typically, 1,3,5-tricyanobenzene (200 mg, 1.306 mmol) and anhydrous zinc chloride (890 mg, 6.530 mmol) were mixed in an agate mortar in a glovebox (99.99% argon with 0.1 ppm water) and transferred into a glass ampule. The ampule was evacuated by vacuum pump, sealed and heated at the rate of 5 °C/min to 400 °C and maintained at this temperature for 40 h. Then the ampule was cooled to room temperature and opened. The inside compound was washed thoroughly with 5% HCl solution, deionized water and tetrahydrofuran, and then dried under vacuum at 120 °C for 12 h to get the dark brown powder.

PTFs. PTFs were synthesized under the similar procedure of m-CTF, but at higher temperatures—550, 600, 650, and 700 °C—in quartz ampules, and the final products were black powders.

Electrochemical Measurements. Electrochemical measurements were performed in a traditional two-electrode symmetric supercapacitor system (a coin-type cell of 2032 size) with room temperature ionic liquid, 1-ethyl-3-methylimidazolium tetrafluoroborate ($EMIMBF_4$) as the electrolyte. Typically, the electrode films were prepared by grinding the PTFs (85 wt%, about 100 mg), carbon black (10 wt%, Super P conductive), and polytetrafluoroethylene (5 wt%, 60% in water, and diluted to 6% before use) in an agate mortar. The electrode film was dried under vacuum at 120 °C for 12 h, and cut to circular tablets with diameter of 12 mm and mass of about 2.5−3 mg. Two tablets with exactly the same mass were pressed onto stainless steel wire meshes (316L, 400 meshes, diameter of 15 mm) respectively as the two symmetric working electrodes. The two electrodes separated by glass fiber film (Whatman) were soaked into $EMIMBF_4$ electrolyte and assembled into a coin-type cell.

CV curves, galvanostatic charge−discharge curves, and Nyquist plots were collected on a CHI660D electrochemical workstation at room temperature. The specific capacitance (C, F/g) was calculated from the slop of discharge curve using the formula: $C = 2It/mV$, where I (unit: A) is the discharge current, m (unit: g) is the mass of PTFs in one electrodes, t (unit: s) is the discharge time, and V (unit: V) is the discharge voltage. The energy densities (E, Wh/kg) were calculated by $E = {}^1/_8 CV^2(1000/3600)$. The power densities ($P$, W/kg) were calculated by $P = E/(t/3600)$.

ASSOCIATED CONTENT

Supporting Information

Experimental details, Figures S1−S10, Table S1−S3, and a video. This material is available free of charge via the Internet at http://pubs.acs.org.

AUTHOR INFORMATION

Corresponding Author

zhilj@nanoctr.cn

Notes

The authors declare no competing financial interest.

ACKNOWLEDGMENTS

The authors acknowledge the support from the Ministry of Science and Technology of China (No. 2012CB933403), the National Natural Science Foundation of China (Grant Nos. 21173057, 21273054, and 51102168), the Sino-German Center for Research Promotion (GZ879), the Eastern Scholar Salon, and the Chinese Academy of Sciences.

REFERENCES

(1) Miller, J. R.; Simon, P. *Science* **2008**, *321*, 651.
(2) Zhai, Y.; Dou, Y.; Zhao, D.; Fulvio, P. F.; Mayes, R. T.; Dai, S. *Adv. Mater.* **2011**, *23*, 4828.
(3) Sun, Y.; Wu, Q.; Shi, G. *Energy Environ. Sci.* **2011**, *4*, 1113.
(4) Simon, P.; Gogotsi, Y. *Nat. Mater.* **2008**, *7*, 845.
(5) Zhang, L.; Zhang, F.; Yang, X.; Leng, K.; Huang, Y.; Chen, Y. *Small* **2013**, *9*, 1342.
(6) Zhu, Y.; Murali, S.; Stoller, M. D.; Ganesh, K. J.; Cai, W.; Ferreira, P. J.; Pirkle, A.; Wallace, R. M.; Cychosz, K. A.; Thommes, M.; Su, D.; Stach, E. A.; Ruoff, R. S. *Science* **2011**, *332*, 1537.
(7) Yang, X.; Zhu, J.; Qiu, L.; Li, D. *Adv. Mater.* **2011**, *23*, 2833.
(8) Sillars, F. B.; Fletcher, S. I.; Mirzaeian, M.; Hall, P. J. *Phys. Chem. Chem. Phys.* **2012**, *14*, 6094.

DOI: 10.1021/ja508693y
J. Am. Chem. Soc. 2015, 137, 219−225

(9) Feng, D.; Lv, Y.-Y.; Wu, Z.-X.; Dou, Y.-Q.; Han, L.; Sun, Z.-K.; Xia, Y.-Y.; Zheng, G.-F.; Zhao, D.-Y. *J. Am. Chem. Soc.* **2011**, *133*, 15148.
(10) Fan, Z.; Yan, J.; Zhi, L.; Zhang, Q.; Wei, T.; Feng, J.; Zhang, M.; Qian, W.; Wei, F. *Adv. Mater.* **2010**, *22*, 3723.
(11) Xie, K.; Qin, X.; Wang, X.; Wang, Y.; Tao, H.; Wu, Q.; Yang, L.; Hu, Z. *Adv. Mater.* **2012**, *24*, 347.
(12) Zhang, L.; Yang, X.; Zhang, F.; Long, G.; Zhang, T.; Leng, K.; Zhang, Y.; Huang, Y.; Ma, Y.; Zhang, M.; Chen, Y. *J. Am. Chem. Soc.* **2013**, *135*, 5921.
(13) Zhang, L.; Zhang, F.; Yang, X.; Long, G.; Wu, Y.; Zhang, T.; Leng, K.; Huang, Y.; Ma, Y.; Yu, A.; Chen, Y. *Sci. Rep.* **2013**, *3*, 1408.
(14) Largeot, C.; Portet, C.; Chmiola, J.; Taberna, P.-L.; Gogotsi, Y.; Simon, P. *J. Am. Chem. Soc.* **2008**, *130*, 2730.
(15) Sillars, F. B.; Fletcher, S. I.; Mirzaeian, M.; Hall, P. J. *Energy Environ. Sci.* **2011**, *4*, 695.
(16) Wen, Z.; Wang, X.; Mao, S.; Bo, Z.; Kim, H.; Cui, S.; Lu, G.; Feng, X.; Chen, J. *Adv. Mater.* **2012**, *24*, 5610.
(17) Wu, Z. S.; Winter, A.; Chen, L.; Sun, Y.; Turchanin, A.; Feng, X.; Mullen, K. *Adv. Mater.* **2012**, *24*, 5130.
(18) Zhang, L. L.; Zhao, X.; Ji, H. X.; Stoller, M. D.; Lai, L. F.; Murali, S.; Mcdonnell, S.; Cleveger, B.; Wallace, R. M.; Ruoff, R. S. *Energy Environ. Sci.* **2012**, *5*, 9618.
(19) Xu, Y.; Lin, Z.; Huang, X.; Wang, Y.; Huang, Y.; Duan, X. *Adv. Mater.* **2013**, *25*, 5779.
(20) Hulicova-Jurcakova, D.; Puziy, A. M.; Poddubnaya, O. I.; Suarez-Garcia, F.; Tascon, J. M. D.; Lu, G. Q. *J. Am. Chem. Soc.* **2009**, *131*, 5026.
(21) Han, J.; Zhang, L. L.; Lee, S.; Oh, J.; Lee, K. S.; Potts, J. R.; Ji, J.; Zhao, X.; Ruoff, R. S.; Park, S. *ACS Nano* **2013**, *7*, 19.
(22) Hall, P. J.; Mirzaeian, M.; Fletcher, S. I.; Sillars, F. B.; Rennie, A. J. R.; Shitta-Bey, G. O.; Wilson, G.; Cruden, A.; Carter, R. *Energy Environ. Sci.* **2010**, *3*, 1238.
(23) Lota, G.; Lota, K.; Frackowiak, E. *Electrochem. Commun.* **2007**, *9*, 1828.
(24) Hulicova-Jurcakova, D.; Kodama, M.; Shiraishi, S.; Hatori, H.; Zhu, Z. H.; Lu, G. Q. *Adv. Funct. Mater.* **2009**, *19*, 1800.
(25) Wang, D. W.; Li, F.; Yin, L. C.; Lu, X.; Chen, Z. G.; Gentle, I. R.; Lu, G. Q.; Cheng, H. M. *Chem.—Eur. J.* **2012**, *18*, 5345.
(26) Lee, Y.-H.; Chang, K.-H.; Hu, C.-C. *J. Power Sources* **2013**, *227*, 300.
(27) Chmiola, J.; Yushin, G.; Gogotsi, Y.; Portet, C.; Simon, P.; Taberna, P. L. *Science* **2006**, *313*, 1760.
(28) Chmiola, J.; Largeot, C.; Taberna, P. L.; Simon, P.; Gogotsi, Y. *Angew. Chem., Int. Ed.* **2008**, *47*, 3392.
(29) Huang, J.; Sumpter, B. G.; Meunier, V. *Angew. Chem., Int. Ed.* **2008**, *47*, 520.
(30) Shim, Y.; Kim, H. J. *ACS Nano* **2010**, *4*, 2345.
(31) Feng, G.; Cummings, P. T. *J. Phys. Chem. Lett.* **2011**, *2*, 2859.
(32) Su, D. S.; Schloegl, R. *ChemSusChem* **2010**, *3*, 136.
(33) Kim, Y. J.; Horie, Y.; Ozaki, S.; Matsuzawa, Y.; Suezaki, H.; Kim, C.; Miyashita, N.; Endo, M. *Carbon* **2004**, *42*, 1491.
(34) Dawson, R.; Cooper, A. I.; Adams, D. J. *Prog. Polym. Sci.* **2012**, *37*, 530.
(35) Thomas, A. *Angew. Chem., Int. Ed.* **2010**, *49*, 8328.
(36) Xu, Y.; Jin, S.; Xu, H.; Nagai, A.; Jiang, D. *Chem. Soc. Rev.* **2013**, *42*, 8012.
(37) Ding, S. Y.; Wang, W. *Chem. Soc. Rev.* **2013**, *42*, 548.
(38) Colson, J. W.; Dichtel, W. R. *Nat. Chem.* **2013**, *5*, 453.
(39) Zhuang, X.; Mai, Y.; Wu, D.; Zhang, F.; Feng, X. *Adv. Mater.* **2014**, DOI: 10.1002/adma.201401857.
(40) Schmidt, J.; Weber, J.; Epping, J. D.; Antonietti, M.; Thomas, A. *Adv. Mater.* **2009**, *21*, 702.
(41) Uribe-Romo, F. J.; Hunt, J. R.; Furukawa, H.; Klöck, C.; O'Keeffe, M.; Yaghi, O. M. *J. Am. Chem. Soc.* **2009**, *131*, 4570.
(42) Feng, X.; Ding, X.; Jiang, D. *Chem. Soc. Rev.* **2012**, *41*, 6010.
(43) Kuhn, P.; Antonietti, M.; Thomas, A. *Angew. Chem., Int. Ed.* **2008**, *47*, 3450.
(44) Zhuang, X.; Zhang, F.; Wu, D.; Forler, N.; Liang, H.; Wagner, M.; Gehrig, D.; Hansen, M. R.; Laquai, F.; Feng, X. *Angew. Chem., Int. Ed.* **2013**, *52*, 9668.
(45) Kuhn, P.; Thomas, A.; Antonietti, M. *Macromolecules* **2008**, *42*, 319.
(46) Wu, D.; Xu, F.; Sun, B.; Fu, R.; He, H.; Matyjaszewski, K. *Chem. Rev.* **2012**, *112*, 3959.
(47) Zhuang, X.; Zhang, F.; Wu, D.; Feng, X. *Adv. Mater.* **2014**, *26*, 3081.
(48) Kou, Y.; Xu, Y.; Guo, Z.; Jiang, D. *Angew. Chem., Int. Ed.* **2011**, *50*, 8753.
(49) Hao, L.; Luo, B.; Li, X. L.; Jin, M. H.; Fang, Y.; Tang, Z. H.; Jia, Y. Y.; Liang, M. H.; Thomas, A.; Yang, J. H.; Zhi, L. J. *Energy Environ. Sci.* **2012**, *5*, 9747.
(50) Hao, L.; Li, X.; Zhi, L. *Adv. Mater.* **2013**, *25*, 3899.
(51) Bojdys, M. J.; Jeromenok, J.; Thomas, A.; Antonietti, M. *Adv. Mater.* **2010**, *22*, 2202.
(52) Ren, S.; Bojdys, M. J.; Dawson, R.; Laybourn, A.; Khimyak, Y. Z.; Adams, D. J.; Cooper, A. I. *Adv. Mater.* **2012**, *24*, 2357.
(53) Katekomol, P.; Roeser, J.; Bojdys, M.; Weber, J.; Thomas, A. *Chem. Mater.* **2013**, *25*, 1542.
(54) Li, X.; Song, Q.; Hao, L.; Zhi, L. *Small* **2014**, *10*, 2122.
(55) Kuhn, P.; Forget, A. l.; Su, D.; Thomas, A.; Antonietti, M. *J. Am. Chem. Soc.* **2008**, *130*, 13333.
(56) Usachov, D.; Vilkov, O.; Grueneis, A.; Haberer, D.; Fedorov, A.; Adamchuk, V. K.; Preobrajenski, A. B.; Dudin, P.; Barinov, A.; Oehzelt, M.; Laubschat, C.; Vyalikh, D. V. *Nano Lett.* **2011**, *11*, 5401.
(57) Li, Z.; Xu, Z. W.; Tan, X. H.; Wang, H. L.; Holt, C. M. B.; Stephenson, T.; Olsen, B. C.; Mitlin, D. *Energy Environ. Sci.* **2013**, *6*, 871.
(58) Simon, P.; Gogotsi, Y. *Acc. Chem. Res.* **2012**, *46*, 1094.
(59) Zheng, C.; Qian, W.; Cui, C.; Zhang, Q.; Jin, Y.; Zhao, M.; Tan, P.; Wei, F. *Carbon* **2012**, *50*, 5167.
(60) Jeong, H. M.; Lee, J. W.; Shin, W. H.; Choi, Y. J.; Shin, H. J.; Kang, J. K.; Choi, J. W. *Nano Lett.* **2011**, *11*, 2472.
(61) Hulicova, D.; Yamashita, J.; Soneda, Y.; Hatori, H.; Kodama, M. *Chem. Mater.* **2005**, *17*, 1241.
(62) Rauda, I. E.; Augustyn, V.; Dunn, B.; Tolbert, S. H. *Acc. Chem. Res.* **2013**, *46*, 1113.
(63) Yun, Y. S.; Cho, S. Y.; Shim, J.; Kim, B. H.; Chang, S. J.; Baek, S. J.; Huh, Y. S.; Tak, Y.; Park, Y. W.; Park, S.; Jin, H. J. *Adv. Mater.* **2013**, *25*, 1993.
(64) Ghaffari, M.; Zhou, Y.; Xu, H.; Lin, M.; Kim, T. Y.; Ruoff, R. S.; Zhang, Q. M. *Adv. Mater.* **2013**, *25*, 4879.
(65) Lei, Z. B.; Liu, Z. H.; Wang, H. J.; Sun, X. X.; Lu, L.; Zhao, X. S. *J. Mater. Chem. A* **2013**, *1*, 2313.
(66) Kim, T.; Kang, H. C.; Tung, T. T.; Lee, J. D.; Kim, H.; Yang, W. S.; Yoon, H. G.; Suh, K. S. *RSC Adv.* **2012**, *2*, 8808.
(67) Wang, H.; Xu, Z.; Kohandehghan, A.; Li, Z.; Cui, K.; Tan, X.; Stephenson, T. J.; King'ondu, C. K.; Holt, C. M.; Olsen, B. C.; Tak, J. K.; Harfield, D.; Anyia, A. O.; Mitlin, D. *ACS Nano* **2013**, *7*, 5131.
(68) Zhang, L. L.; Zhao, X.; Stoller, M. D.; Zhu, Y.; Ji, H.; Murali, S.; Wu, Y.; Perales, S.; Clevenger, B.; Ruoff, R. S. *Nano Lett.* **2012**, *12*, 1806.
(69) Jung, N.; Kwon, S.; Lee, D.; Yoon, D. M.; Park, Y. M.; Benayad, A.; Choi, J. Y.; Park, J. S. *Adv. Mater.* **2013**, *25*, 6854.
(70) Hao, G. P.; Lu, A. H.; Dong, W.; Jin, Z. Y.; Zhang, X. Q.; Zhang, J. T.; Li, W. C. *Adv. Energy Mater.* **2013**, *3*, 1421.
(71) Lin, Q.; Wu, T.; Zheng, S.-T.; Bu, X.; Feng, P. *J. Am. Chem. Soc.* **2011**, *134*, 784.

DOI: 10.1021/ja508693y
J. Am. Chem. Soc. 2015, 137, 219−225